Part One
Multiphoton Imaging and Nanoprocessing

Laser Imaging and Manipulation in Cell Biology. Edited by Francesco S. Pavone
Copyright © 2010 WILEY-VCH Verlag GmbH & Co. KGaA, Weinheim
ISBN: 978-3-527-40929-7

1
Multiphoton Imaging and Nanoprocessing of Human Stem Cells

Karsten König and Aisada Uchugonova

1.1
Introduction

Two-photon microscopy and multiphoton tomography with near-infrared (NIR) femtosecond lasers has revolutionized high-resolution live cell imaging [1].

Marker-free, non-destructive long-term monitoring of cells and tissues under native physiological conditions became possible. Nowadays, optical biopsies provide even better images than sliced and fixed physical biopsies [2].

Interestingly, femtosecond laser devices operating at up to three orders higher transient laser intensities than in two-photon microscopes can be used as highly precise nanoprocessing tools without collateral effects. This enables optical cleaning of cell clusters and targeted transfection of plant cells, animal cells, and human cells.

This chapter focuses on the usage of multiphoton technology for the investigation of human stem cells, one of the most interesting objects of cell biology, developmental biology, nanobiotechnology, and modern medicine.

The Russian histologist Maximow predicted the existence of stem cells 100 years ago [3]. In the 1950s, stem cells in mouse bone marrow were discovered [4]. Stem cell therapy was first demonstrated on patients with leukemia by the Nobel Prize winner Thomas at MIT in 1956. Nowadays, hematopoietic and bone marrow stem cell transplantation have become the standard therapy to treat patients with leukemia and lymphoma in combination with chemo- and ionizing radiation-therapy. There is a hope that within the next few years stem cells can be used to treat Parkinson's, Alzheimer's, cancer, diabetes, and heart diseases. In addition, stem cells will be employed to engineer tissues and to synthesize novel pharmaceutical components.

Stem cells can be classified into embryonic stem cells (ESCs) and tissue specific/adult stem cells. ESCs were isolated from mouse in 1981 [5, 6] and from humans in 1998 [7]. In 2009, the world's first human clinical trial of ESC-based therapy was approved by the American Food and Drug Administration on patients with spinal cord injuries (Geron Corp., Menlo Park, CA, USA; www.geron.com).

Laser Imaging and Manipulation in Cell Biology. Edited by Francesco S. Pavone
Copyright © 2010 WILEY-VCH Verlag GmbH & Co. KGaA, Weinheim
ISBN: 978-3-527-40929-7

So far, stem cells have to be characterized and sorted by methods that require exogenous probes and that are often destructive in 1984. It is of great interest to develop non-destructive, marker-free *in vivo* techniques to detect and to manipulate stem cells.

Multiphoton imaging is the ideal technique to trace and image the stem cells over a long period of time as well as to study their differentiation process without any marker. Furthermore, multiphoton technology can be used for optical cleaning and optical DNA transfer into stem cells. This chapter focuses on multiphoton technology for human stem cell research.

1.2 Principle of Two-Photon Microscopy and Multiphoton Tomography

Confocal one-photon (linear) microscopy was invented by Marvin Minsky in 1957. With the availability of lasers, beam scanning systems, and sensitive photomultipliers (PMT), the first commercial confocal laser scanning microscopes (CLSMs) for 3D imaging became available in the 1980s. ZEISS Jena and the University of Jena built a confocal picosecond laser scanning microscope with temporal and spatial resolution in 1988 [8–10]. Thousands of CLSMs are currently operating in the field of life sciences, mainly based on one-photon excited fluorescence where the visible (VIS) intracellular fluorescence of exogenous molecular and cellular probes is detected with submicron resolution. Optical sectioning enables the 3D reconstruction of the object of interest.

Conventional one-photon fluorescence microscopes employ UV and VIS light sources, such as the argon-ion laser at 364/488/515 nm emission, the frequency-converted Nd:YAG laser at 355/532 nm, and the helium neon laser at 543/633 nm. Typically, the fluorescence excitation power on the target is some microwatts, which corresponds to light intensities in the range of $kW\,cm^{-2}$ when focused to diffraction-limited spots by objectives with high numerical aperture (NA $>$ 1).

Wilson and Sheppart proposed the application of nonlinear excitation to microscopy in 1984. Denk, Strickler, and Webb realized, finally, the first two-photon NIR microscope based on a femtosecond dye laser in 1990 [1]. Multiphoton absorption requires high light intensities in the range $100\,MW\,cm^{-2}$ up to $TW\,cm^{-2}$. In principle, continuous wave (CW) NIR radiation can induce two-photon effects if the power exceeds 100 mW and when high NA objectives are used [11–13]. To avoid trapping effects and to reduce the mean power, most multiphoton microscopes are based on femtosecond laser pulses at MHz repetition rate with high kilowatt peak power (P) and low mean power in the μW/mW range. The multiphoton efficiency of an n-photon process follows a P^n relation. In the case of two-photon microscopy, the two-photon effect depends on P^2/τ. The shorter the pulse width (τ) and the higher the laser power the more fluorescence photons and the better the nanoprocessing. Multiphoton microscopy at a fast scanning rate with microsecond beam dwell times per pixel is possible. Figure 1.1 demonstrates the principle of two-photon microscopy where two NIR photons are absorbed simultaneously to induce a single VIS fluorescence photon.

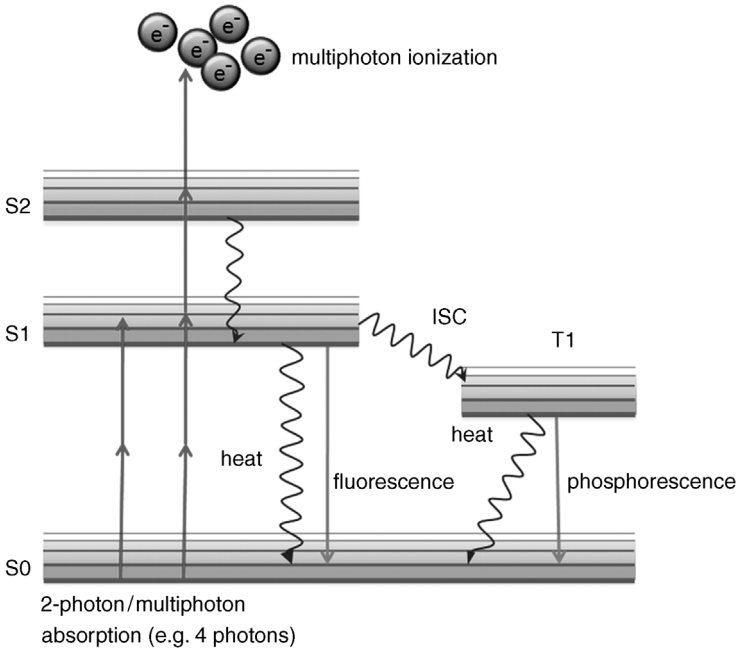

Figure 1.1 Principle of two-photon excited fluorescence at GW cm^{-2} intensities and principle of multiphoton ionization, which requires multiple photons (e.g., 4 or 5) and TW cm^{-2} intensities.

Multiphoton microscopes, including two-photon and three-photon fluorescence microscopes, second-harmonic generation (SHG) and third-harmonic generation (THG) microscopes as well as nanoprocessing microscopes, are based on the application of low energy photons in the NIR between 700 and 1200 nm. This spectral range is also referred as an "optical window" where the one-photon absorption coefficients and scattering coefficients of unstained cells and tissues are low. Most cells (except erythrocytes and melanocytes) appear transparent. The light penetration depth in tissue in this spectral region is high and in the range of some millimeters.

A significant advantage of multiphoton high NA microscopy compared to conventional one-photon microscopy is the tiny sub-femtoliter excitation volume. Absorption in out-of-focus regions is avoided because the probability of two-photon absorption decreases nearly with the distance d from the focal point according to a d^{-4} relation.

In particular, when studying 3D objects, including cell clusters, embryos, and tissues by optical sectioning, multiphoton microscopy is the superior method compared to one-photon confocal scanning microscopy with its large excitation cones and the subsequent problem of out-of-focus damage as well as the disadvantage of using high-energy excitation photons.

Long-term studies have demonstrated that multiphoton microscopy can be performed without photodamage under certain conditions. In particular, single

hamster ovarian cells have been femtosecond laser-exposed for hours with a high 200 GW cm^{-2} peak intensity without any impact on cellular reproduction and vitality [14]. In another long-term study, living hamster embryos were exposed for 24 h with a multiphoton NIR microscope and implanted in the mother animal without impact on embryo development in contrast to control studies performed with a conventional one-photon CW VIS laser microscope [15].

The first commercial multiphoton tomograph, DermaInspect™ (JenLab GmbH), is in clinical use for melanoma diagnosis and *in situ* intradermal drug targeting. It was shown that this femtosecond laser system is safer than conventional UV light sources used in the cosmetic industry and in tanning studios [16].

In addition to conventional one-photon microscopes, multiphoton microscopes enable SHG and THG imaging. In SHG, two photons interact simultaneously with non-centrosymmetrical structures such as collagen and generate coherent radiation at exactly half of the excitation wavelength in forward direction. There is no light absorption. Therefore, photobleaching and photodamage are excluded. SHG enables deep 3D imaging due to backscattered light.

Multiphoton microscopes do not require confocal units or de-scanned detection systems due to the sub-femtoliter excitation volume.

1.3 Multiphoton Microscopes and Multiphoton Tomographs

Owing to patent and marketing issues, most commercial two-photon microscopes are based on expensive confocal microscopes with the extension of a NIR femtosecond laser combined with a special interface. This makes the two-photon microscopes of the major microscope suppliers very expensive and avoids the sale of more compact pinhole-free two-photon microscopes. With the end of patent rights in 2009/2010, low-price ultracompact two-photon systems will become available.

Figure 1.2 shows two-photon microscopes. The first is the ZEISS META-LSM510-NLO confocal microscope (Figure 1.2a). The second is the pinhole-free ultracompact laser scanning microscope "Two-photon TauMap" where the galvoscanners and the photon detectors were attached to the side ports of an inverted microscope (JenLab GmbH, Jena, Germany).

In most microscope systems, compact solid-state "turn-key" tunable 80/90 MHz titanium:sapphire lasers such as the "Chameleon" from Coherent, USA, and "MaiTai" from Newport/Spectra Physics, USA, are employed. The laser beam is typically transferred to a beam expander, a beam attenuator, the scanning optics, x/y-galvoscanner, and focused into the target by a piezo-driven objective of high numerical aperture (NA $>$ 1). The signal is typically measured by a sensitive photomultiplier (PMT).

Exogenous fluorescent probes with high fluorescence quantum yields (e.g., DAPI and Hoechst) require a mean power of 25 to 100 μW at a frame rate of 1 Hz (512 $\times$ 512 pixels). The endogenous intracellular fluorophore NAD(P)H can be imaged with less

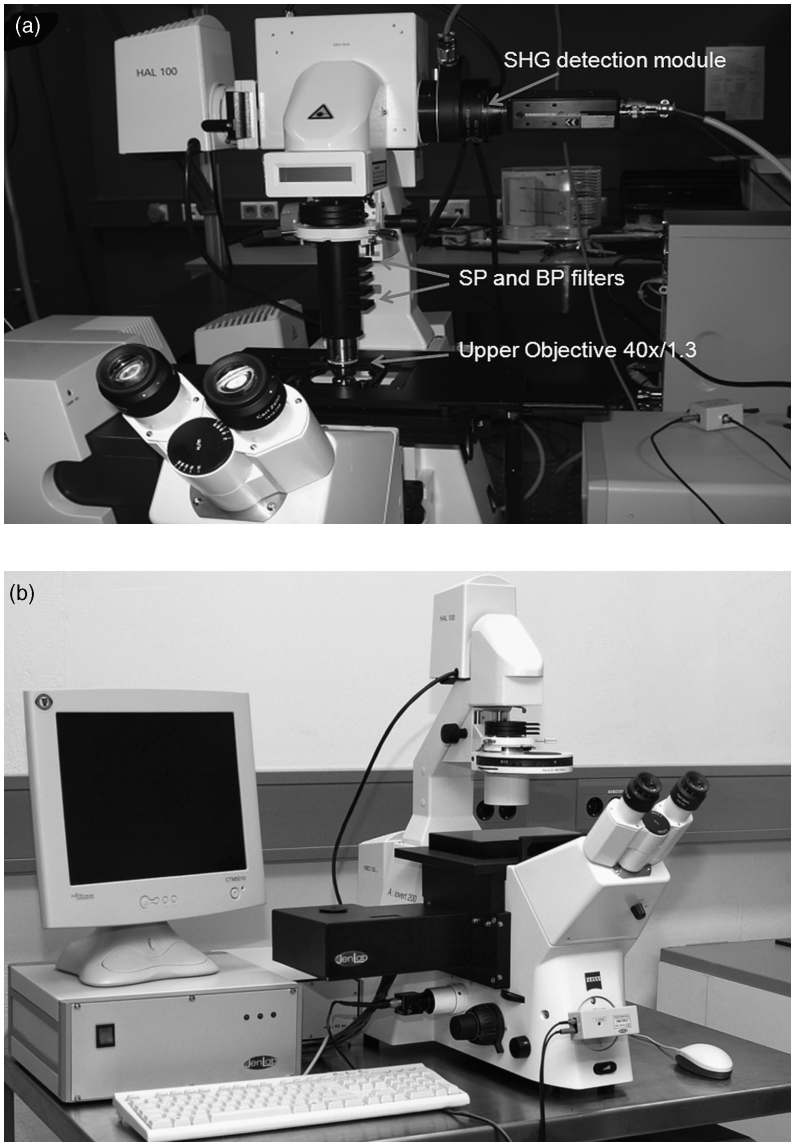

Figure 1.2 Photographs of a ZEISS META LSM510-NLO system with an additional SHG detection module (a) and a compact Two-photon TauMap Microscope (b).

than 2 mW mean power at appropriate NIR wavelengths with typical exposure times of 1 to 8 s per frame.

Optical dispersion results in pulse broadening during transmission through the microscope. Typically, the pulse width at the sample is about 150–300 fs.

Recently, the ultracompact nanoprocessing microscope FemtOgene™ (JenLab GmbH, Jena, Germany) with the shortest femtosecond laser pulses at the target of 12

femtoseconds was released onto the market. The ultrashort pulse width was achieved by dispersion pre-compensation of the whole microscope, including the beam expander, the polarizer for beam attenuation, the tube lens, the objective, filters, and so on, using chirped mirror technology (Figure 1.3).

The microscope can be used in the two-photon fluorescence excitation mode at mean powers in the microwatt range for nondestructive imaging of the stem cell of interest and to monitor the biosynthesis of fluorescent proteins. Furthermore, it can be employed for nanoprocessing when operating in the milliwatt power range in three exposure modes: (i) scanning of a region of interest (ROI) for ablation, (ii) line scanning for cutting, and (iii) single point illumination for drilling where the galvoscanners are fixed to a point of interest.

Nowadays, femtosecond laser tomographs for high-resolution deep-tissue imaging in animals and humans are operating as CE-marked medical devices in Europe, Asia, and Australia. Figure 1.4 shows the two types of multiphoton tomographs DermaInspect and MPTflex™ that are currently available on the market. They are employed for small animal studies based on the detection of fluorescent proteins as well as tissue engineering and for clinical studies regarding skin cancer diagnosis, wound healing studies, and nanoparticle tracking.

1.4
Endogenous Cellular Fluorophores and SHG Active Biomolecule Structures

Non-invasive multiphoton NIR microscopes [1, 14, 17, 18] have been applied to image living single cells and different tissues with a high spatial resolution without any staining. Two-photon autofluorescence can be obtained from intrinsic fluorophores such as NAD(P)H, flavins, porphyrins, elastin, and melanin [19]. In addition, SHG images can be obtained from certain biomolecule structures such as collagen and myosin [15, 20–24].

The most important endogenous cellular fluorophores for two-photon imaging are the reduced coenzymes nicotinamide adenine dinucleotide (NADH) and nicotinamide adenine dinucleotide phosphate (NADPH), referred as NAD(P)H, with a broad emission in the blue/green spectral range. The oxidized form NAD(P) shows no significant VIS fluorescence. The reduced coenzymes possess a folded and an unfolded configuration, with the unfolded ones to bound NAD(P)H. The emission maximum of the unfolded configuration shows a blue-shifted maximum (450 nm) and a higher fluorescence quantum yield than free NAD(P)H with its maximum at 470 nm [19]. The hydrogen-transferring pyridine coenzymes are mainly located in the mitochondria and play a key role in respiratory chain activity and act as sensitive indicators of the cellular metabolism since the metabolic activity of cells is given by the ratios of the concentrations of free to protein-bound NAD(P)H and of NAD(P)H to flavins [19, 25–27]. Normally, the excitation of NAD(P)H requires UV light at around 340 nm. However, the use of UV exposure should be avoided due to photoinduced cytotoxic reactions and the limited light penetration depth.

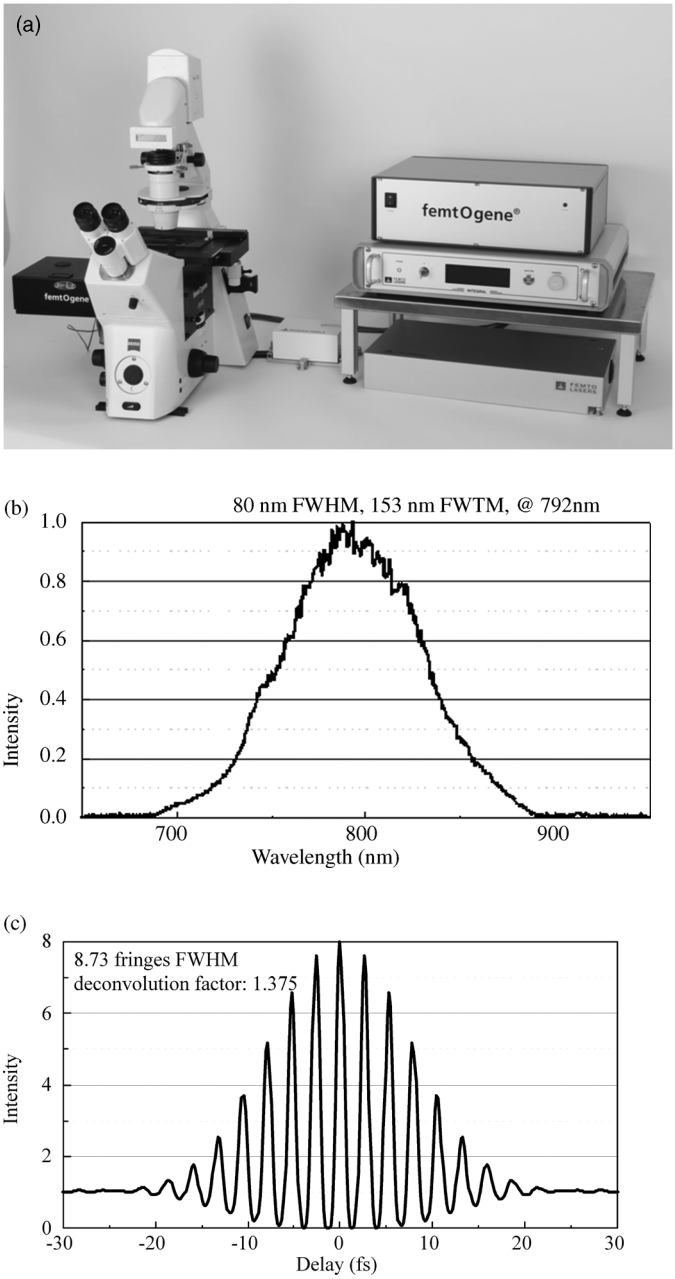

Figure 1.3 Photograph of the imaging and nanoprocessing 12-femtosecond laser microscope Femtogene (a) as well as a spectrum (b) and autocorrelation function at the focus of the 40 ×, NA1.3 objective (c).

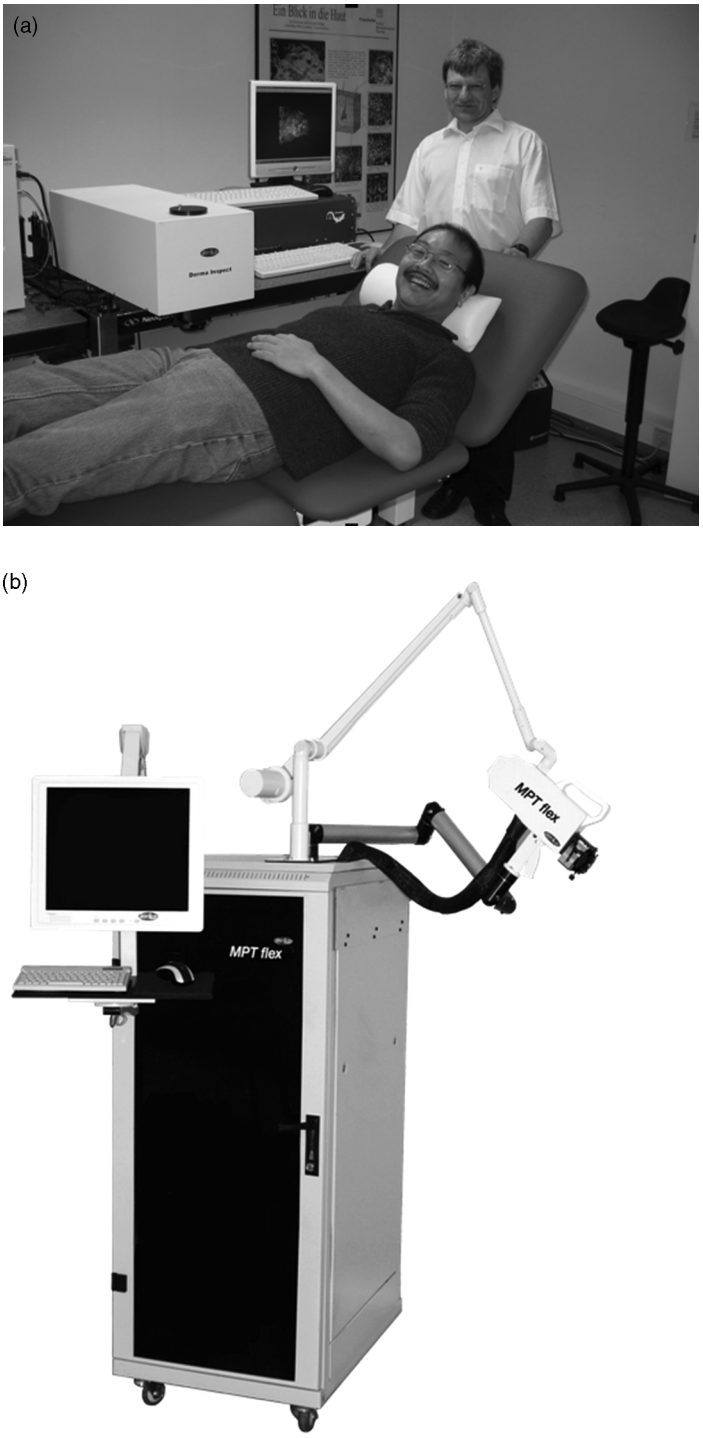

Figure 1.4 Photographs of the multiphoton tomographs DermaInspect (a) and MPTflex (b).

Two-photon NIR excitation is the ideal method to image intracellular/intratissue NAD(P)H without the disadvantages of UV microscopy.

Cellular flavins such as flavin adenine dinucleotide (FAD), flavin mononucleotide (FMN), lipoamide dehydrogenase (LipDH), riboflavin, and electron transfer flavoprotein (ETF) are also fluorescent coenzymes that are involved in oxidation–-reduction reactions [26]. The excitation spectra of these flavins/flavoproteins possess major electronic transitions at 260, 370, and 450 nm as well as an emission peak around 530 nm. The fluorescence intensity decreases when covalently attached to proteins ("flavoprotein," [19]).

Besides the measurement of the fluorescence/SHG/THG intensity by optical sectioning (3D imaging), fluorescence lifetime imaging (FLIM, 4D) and spectral imaging (5D) can be performed. In particular, the arrival times of the fluorescence photons with respect to the excitation time of the molecule and the particular location (pixel) can be determined by time-correlated single photon counting (TCSPC) and the use of photomultipliers with short rise time. When using a PMT array in combination with a polychromator, the "color" of the emitted photon per pixel can be also determined (spectral imaging). Recent developments involve PMT arrays with fast picosecond rise time in combination with a polychromator or other wavelength-selective components to realize spectral FLIM within one scan [28].

1.5
Optical Nanoprocessing

1.5.1
Principle and Mechanism of Femtosecond Laser Nanoprocessing

Femtosecond laser microscopes can be used as precise nanoscissors based on multiphoton ionization at TW cm^{-2} intensities. The simultaneous absorption of several photons, for example, five photons, induces ionization of molecules and the generation of free electrons. The onset of plasma occurs if a density of 10^{21} electrons cm^{-3} is achieved [29]. In the case of water, a "bandgap" of 6.5 eV has to overcome. Since 800-nm photons have a photon energy of 1.55 eV, five photons are required for multiphoton ionization of water molecules [29]. The application of 750-nm photons (1.65 eV) requires four photons. The formation of plasma in aqueous solution results in the formation of plasma-filled cavitation bubbles that can be video-imaged. Interestingly, nanoprocessing of cells can be performed at thresholds below the threshold for multiphoton ionization of water.

The bubbles expand and can induce an implosion combined with destructive jet streams and shock waves. These photodisruptive effects result in destruction of the microenvironment. The onset of photodisruptive effects depends on the transient laser intensity whereas the amount of damage depends on the pulse energy. The smaller the applied pulse energy the smaller the photodisruptive effects [30]. Therefore, low pulse energies are required to perform nanoprocessing without collateral destructive effects. The procedure should, consequently, be performed

near the threshold of multiphoton ionization and plasma formation of cellular structures. This can be realized by fine-tuning of the laser power. In early studies on chromosome cutting, pulse energies of about 1 nJ were applied when using 200–300-femtosecond laser pulses at 80 MHz repetition rate [31]. Precise laser nanosurgery depends on laser wavelength, laser intensity, pulse duration, repetition rate, and irradiation time.

The first femtosecond laser subcellular nanosurgery was demonstrated by König's group in 1999 by dissections of single chromosomes in living cells [31–34]. The group also introduced femtosecond laser assisted single cell transfection by creating transient holes in the cellular membrane [35]. Femtosecond laser pulses have been applied to dissect single dendrites and cytoskeletons, to optically knock out intracellular mitochondria [36–38], for membrane and microtubules surgery [39], and for ocular refractive surgery [40].

1.5.2 Stem Cells

Adult stem cells, also termed somatic or tissue specific stem cells, can be found among differentiated cells within fully developed tissues in a low abundance. For example, mesenchymal stem cells represent 0.01–0.0001% of the total population of nucleated cells in the bone marrow [41, 42]. Mesenchymal stem cells have been also isolated from bone, skin, muscle, adipose, cartilage, peripheral, and umbilical cord blood, whereas hematopoietic stem cells have been isolated from peripheral and umbilical cord blood as well as bone marrow. Neural stem cells have been isolated from different parts of the brain. Stem cells were found in children's primary teeth, hairs, retina, skin, lung, liver, and glands.

Adult stem cells are "multipotent" and differentiate mainly into several specialized cell types depending on the kind of tissue they have been originated from. However, several studies have also shown that cells originated from the mesoderm (muscle, blood, bone, fat) can produce cells normally originated from the endoderm (gut, lungs, liver, and pancreas) and the ectoderm (skin, nervous system) germ layer. Under laboratory conditions, directed differentiation can be induced by the stimulation of certain factors such as the growth factor TGF-β and cytokines. Nanostructures, mechanical stress and vibration, temperature, light, and electrical fields can also induce differentiation [43–46]. The proliferation and differentiation capacity of adult stem cells is limited because they stop dividing after several passages due to a decrease of the telomerase activity and telomere shortening [47–49]. Furthermore, a prolonged culture of adult stem cells can induce tumorogenity [50]. Freshly isolated adult stem cells do not show a propensity for tumor formation. Undesired differentiation occurred under laboratory conditions [51].

More than 2000 patients with Parkinson's disease, Alzheimer's disease, cerebral palsy, diabetes mellitus, spinal cord injury, and cardiac infarction have been successfully treated with autologous adult stem cells from bone marrow in Germany (X-Cell Center at the Institute of Regenerative Medicine, Germany; www.xcell-center.de).

No side effects have been reported. However, the exact repair phenomenon remains to be understood. It would be helpful to trace individual stem cells in culture as well as *in vivo* to study their interaction with the microenvironment over a long period of time. Unfortunately, so far it is difficult to identify, to isolate, and to purify adult stem cells from the tissues.

Embryonic stem cells can be grown in their non-differentiated state for many generations. They can produce cells from the three germ layers, including germ cells under laboratory conditions. The high potential of ESCs to treat diseases has been tested on animal models successfully. Fewer studies have been conducted on human ESCs because of ethical constraints. A tumorogenity of ESCs has been reported upon transplantation [52]. Therefore it is recommended to differentiate cells before transplantation.

Tissue engineering from the patient's own cells is a further major application field that would overcome the problems of the transplanted purely artificial and mechanical prosthesis that cannot display physiological function and missing self-repair. So far various tissues/organs like bladder, blood vessels, skin, cartilage, heart valve, kidney, liver, salivary glands, pancreas, ear, and bone have been generated by tissue engineering and clinical trials have been conducted [53].

Stem cells can be genetically modified for stem cell therapy and the development of specific cell populations. Owing to the restriction of the isolation of ESCs from blastocytes, there is an interest in producing ESC-like cells from somatic cells through reprogramming and nuclear transfer. In 2007, it was demonstrated that induced pluripotent stem cells can be generated from adult dermal fibroblasts by introducing the four genes Oct3/4, Sox2, Klf4, and c-Myc [54].

To find stem cells in tissues, biopsies have to be taken, sliced into microsections, and tagged with the marker. Typically, fluorophores with a high quantum yield are employed in this immunocytochemistry approach where the stem cells are no longer alive. The genetic approach requires procedures to gain, to amplify, and to stain DNA that also destroy the stem cells.

Fluorescence-assisted cell sorting (FACS, a special type of flow cytometry) can be applied to identify and isolate living stem cells in suspension. Hundreds of thousands of cells marked within a fast jet stream pass a laser beam that induces fluorescence from the cells only that are tagged with specific fluorescent stem cell markers. When fluorescence occurs (selection criteria), an electromagnetic field is switched on that charges the fluorescent cell. This particular cell within a droplet can be deflected by a strong electrostatic field and can be collected. FACS enables precise counting and accurate sorting of stem cells of interest. The major disadvantages of FACS are the low viability of sorted cells.

In view of the various disadvantages of the different identification and sorting techniques, it would be of great importance to find chemical-free methods to identify stem cells in their native 3D tissue environment as well as in *in vitro* cell suspensions and biopsies. It would also be of tremendous interest if a marker-free imaging method could be employed to monitor stem cells and their differentiation over a long period of time under physiological conditions.

1.5.3 Upgrading the Multiphoton Microscope

Three-dimensional multiphoton microscopy (x,y,z) is based on optical sections in different tissue depths. One section is obtained by beam scanning using a fast x–y galvoscanner in a typical 512×512 pixel field covering an area of $230 \times 230\,\mu m^2$ at 25.6 µs pixel dwell time. To change the focal plane either the motorized stage can be moved in the axial (z) direction (ZEISS LSM510-NLO) or the focusing optics is moved by a piezosystem (FemtOgene, Two-photon TauMap, MIPOS 5, 500 µm working distance, Piezosystems Jena, Germany). 3D images are obtained by the correlation of the PMT signal with the position of the x–y galvoscanners and the z-position of the stage/focusing optics. The microscope can be upgraded to a fourth dimension system (4D microscopy: x,y,z,τ), which depicts the fluorescence lifetime as false color into the high-resolution image.

Upon photoexcitation, within femtoseconds from the ground state (S_0) to a higher electronic state (S_1), the molecule will remain in the excited state only transiently for some picoseconds up to tens of nanoseconds. This average time a fluorescent molecule remains in the excited state is referred to as the "fluorescence lifetime, τ." The parameter τ is a signature of the fluorescent material and independent of the concentration, illumination intensity, light path of the optical system, and detector [55]. The fluorescence lifetime depends on the microenvironment and changes as a result of the interaction with other molecules due to the loss of their excited state energy by additional decay pathways.

Since its introduction to life sciences 20 years ago [9, 10], fluorescence lifetime imaging microscopy (FLIM) has become a key technique for imaging cellular processes, protein–protein interactions, and tissue compartments [56, 57].

The fluorescence lifetime is often determined by time-correlated single photon counting (TCSPC) where the arrival times of photons are measured with respect to the excitation pulse. Thousands of photons are counted per pixel and placed into different "time channels" to build up a histogram and a fluorescence decay curve, $F(t) = F_0 e^{-t/\tau}$, respectively. The fluorescence lifetime can be calculated from this decay curve with an accuracy according to Poisson statistics [55]. Often, the fluorescence decay curve represents a multi-exponential decay due to the presence of different fluorescent molecules in one "pixel" or the presence of one fluorophore in its free and its bound form. Typical fitting procedures can consider a mono-exponential as well as a bi-exponential behavior, $F(t) = A_1 e^{-t/\tau_1} + A_2 e^{-t/\tau_2}$.

Sometimes, the intensities and the fluorescence lifetimes of two different fluorophores are similar. It would be helpful to have a further criterion to distinguish between them. This can be the "color" of the emitted photon, which can be determined by separation of the photons into "spectral channels." The method is also called "emission fingerprinting" [58]. The combination with 4D microscopy enables "spectral FLIM" (5D microscopy: x,y,z,τ,λ). Spectral imaging can be performed, for example, with a 32-channel PMT array (ZEISS-META, Hamamatsu) in combination with a polychromator with a resolution of 10.5 nm per channel. A full 512×512 lambda stack of data from all 32 channels (the full visible spectrum

382–714 nm) can be acquired in 0.8 s. In addition, a further fast PMT can be used for FLIM. More elegant is the employment of an array with fast PMTs in combination with a polychromator as well as a multichannel FLIM module such as the SPC830 from Becker & Hickl GmbH, which collects the photons according to the arrival time as well as their color.

1.5.4
Autofluorescence Imaging of Human Stem Cells

Two-photon excitation of endogenous fluorophores enables non-destructive high resolution imaging of living cells and extracellular matrix (ECM) components over a long period of time. The application of NIR femtosecond laser pulses induced a blue/green cellular autofluorescence that provided information on the cell morphology and cell size as well as enabled visualization of some cell structures and ECM components with submicron resolution without exogenous markers. The most intense fluorescent structures were found to be the mitochondria. Table 1.1 shows typical laser and exposure parameters for safe stem cell imaging with either the ZEISS LSM510-NLO microscope with 250 fs pulse width at the target and a preferred excitation wavelength of 750 nm or the ultracompact FemtOgene 12-fs microscope. Figure 1.5 demonstrates autofluorescence images of human salivary gland stem cells (hSGSCs), human dental pulp stem cells (hDPSCs), and human pancreatic stem cells (hPSC) acquired at 750 nm excitation wavelength. The ellipsoidal/round non-fluorescent nucleus and the fluorescent mitochondrial network are clearly seen.

When using 750 and 800 nm, NAD(P)H as well flavins/flavoproteins have been efficiently excited by a two-photon process. When changing to 850 nm or even 900 nm, flavins/flavoproteins (e.g., FAD) only and not NAD(P)H were efficiently excited.

Spectral measurements showed a fluorescence maximum at 460–470 nm when excited with 750 nm light, which is consistent with the emission behavior of free and protein bound NADH. The maximum shifted to 530–535 nm when using 900 nm light, which is consistent with flavin emission (Figure 1.6).

Spatially resolved autofluorescence decay curves were obtained at 750 and 900 nm and a scanning time of up to 30 s per frame. Figure 1.7 represents a typical FLIM image, a histogram, and a particular intramitochondrial fluorescence decay curve of 750 nm-excited hSGSC stem cells based on 6740 detected photons. The bi-exponential fit with the optimal fitting parameter $\chi^2 = 1.00$ revealed a fast decaying fluorophore with a short lifetime τ_1 of 0.17 ns and an amplitude $a_1 = 72\%$ and a second component with $\tau_2 = 1.8$ ns and $a_2 = 28\%$. Although the amplitude is lower, the longer component provides $\tau_2 a_2 / \tau_1 a_1 = 4$ times more fluorescence intensity than the short-lived fluorophore.

1.5.5
Multiphoton Imaging during Differentiation

Human SGSCs stem cells can undergo adipogenic differentiation resulting in the formation of mature adipocytes.

Table 1.1 Typical laser parameters and exposure parameters used for two-photon imaging of stem cells.

Pulse width, τ (fs)	Mean power, P (mW)	Wave length, λ (nm)	Spot size, d (µm)	Repetition frequency, f (MHz)	Pulse energy, E (pJ)	Peak power, P_{max} (kW)	Mean light intensity, I (MW cm^{-2})	Peak light intensity, I_{peak} (GW cm^{-2})	Exposure time, t (µs)	Energy density (J cm^{-2})	Laser pulse number, n	Applied energy (nJ)
250 (LSM 510)	5	750	0.58 (NA 1.3)	80	62.5	0.25	1.9	95	6	11.4	480	30
12 FemtOgene	0.5	800	0.62 (NA 1.3)	75	6.6	0.55	0.2	182	6	1.2	450	3

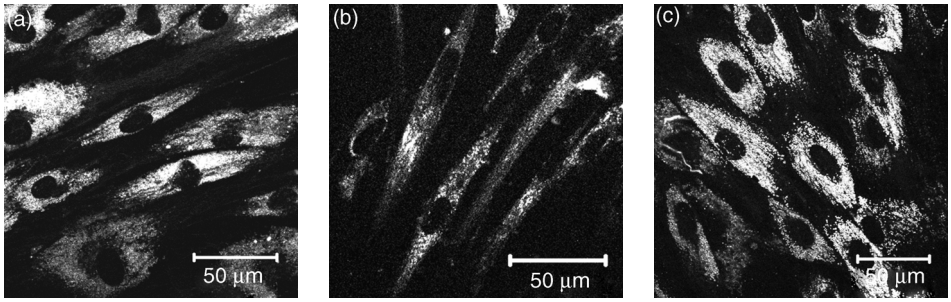

Figure 1.5 Two-photon autofluorescence images of human stem cells excited at 750 nm. (a) Human salivary gland stem cells, (b) human dental pulp stem cells, and (c) human pancreatic stem cells [59].

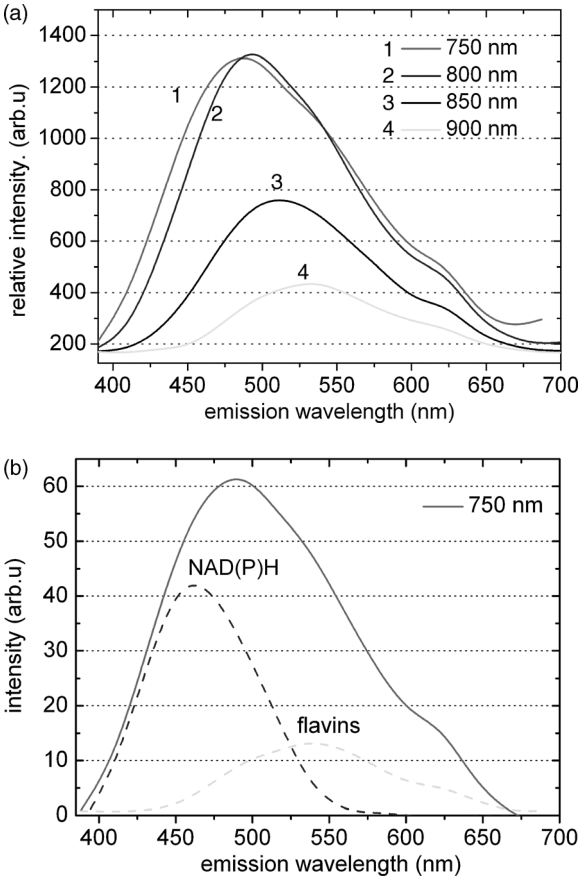

Figure 1.6 Spectral measurement of hSGSC stem cells. (a) Four excitation wavelengths were employed. The emission peak shows a redshift with increasing excitation wavelength due to the preferred two-photon excitation of flavins versus NAD(P)H. (b) The 750/800 nm excited emission spectra can be considered as an overlay of the two fluorophores NAD(P)H and flavins (dotted lines, spectral unmixing).

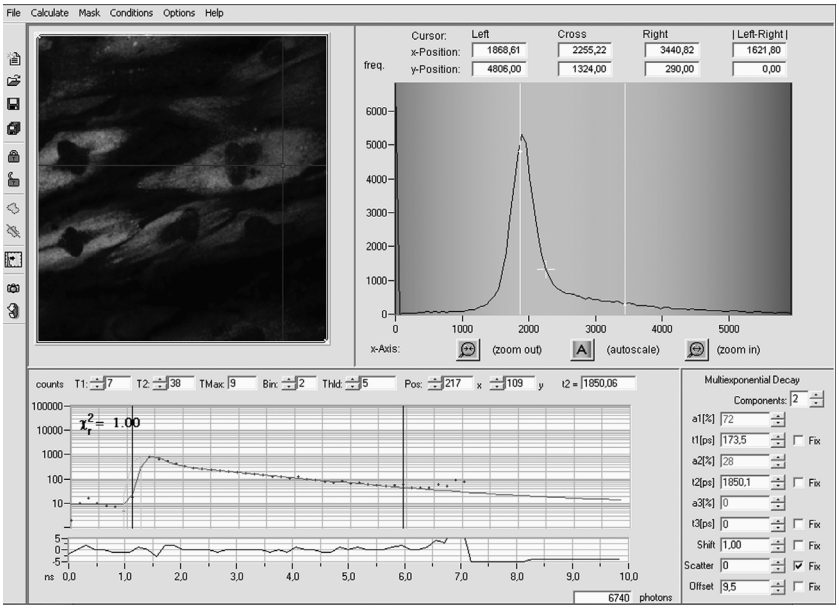

Figure 1.7 False-color FLIM image of hSGSC stem cells. The depicted decay curve is from an intracellular pixel of the right cell (cross), the τ_2-histogram from the whole frame [59].

Figure 1.8 shows images of about ten stem cells inside a spheroid originated from hSGSC stem cells taken one week after administration of adipogenic differentiation factors. Two cells are differentiated into about 100-µm long adipocytes with mainly round, non-fluorescent lipid vacuoles with a diameter up to 10 µm that store fat. When analyzing the gray levels of the autofluorescence pattern, the differentiated cells were found to possess lower fluorescence intensity than cells without fat droplets. Spectral imaging at 750 nm excitation wavelength revealed significant changes of the emission spectrum. Non-differentiated highly-fluorescent cells exhibited a maximum at 490 nm with shoulders at 540 and 620 nm, whereas the adipocytes emitted at 460 nm with a less pronounced shoulder at 620 nm. The maximum at 460 nm corresponds to the typical emission maximum of NAD(P)H. FLIM data from highly fluorescent vacuole-free stem cells revealed a τ_m of 0.59 ns, a short 0.22 ns decay component (78%), and a long 1.93 ns decay component. In contrast, the mean lifetime of cells with fat droplets was much longer with typical values of more than 0.85 ns.

In addition to two-photon excited fluorescence, two-photon microscopy allows the detection of SHG in particular from the ECM component collagen. Collagen also shows weak autofluorescence. When using excitation wavelengths shorter than 800 nm, SHG cannot be detected due to technical reasons (UV absorbing filters). The 750-nm-excited autofluorescence decays reveal a short component of about 0.26 ns lifetime with an amplitude of 58% whereas the longer component has a lifetime of 2.6 ns (42%). By contrast, the signal is mainly based on SHG (98%) when

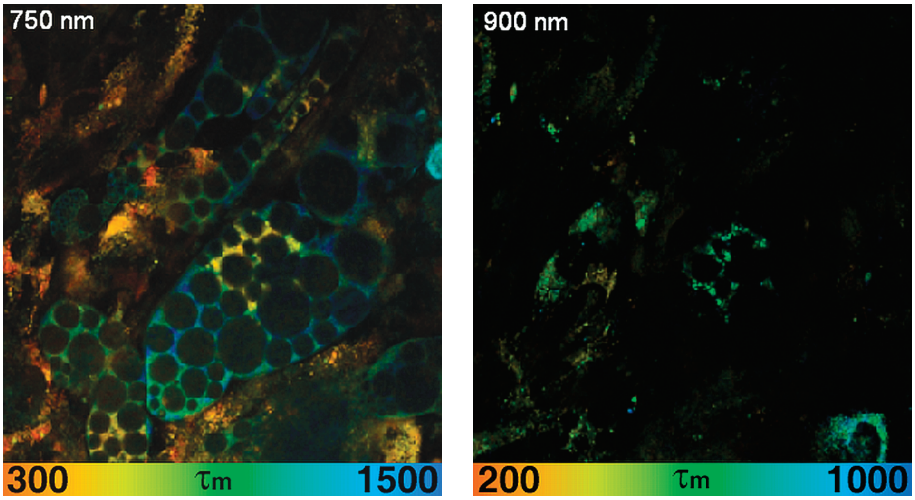

Figure 1.8 False-color coded τ_m FLIM images of cells excited at 750 and 900 nm, respectively, after adipogenic differentiation. At the higher excitation wavelength, no NAD(P)H fluorescence is observed.

using an excitation wavelength of 850–900 nm. Therefore, false-color coded FLIM images can be used to differentiate between SHG and autofluorescence (Figure 1.9). The biosynthesis of collagen in 3D salivary gland and pancreatic stem/progenitor spheroids has been monitored after incubation in the chondrogenic differentiation medium. The differentiation process has been observed for a long time period (up to 5 weeks). The first SHG signal was detected eight days after the introduction of the stimulating agents.

In addition, SHG radiation was detected in the case of osteogenic differentiation from pancreatic, salivary gland, and bone marrow mesenchymal stem cells.

1.5.6 Nanoprocessing

The sub-20 fs microscope FemtOgene, as well as the 250 fs ZEISS laser scanning microscopes, can perform nanoprocessing by single point illumination and line scanning at mW mean powers. Sub-20 fs laser pulses required significant less power than the long 250 fs laser pulses. In fact, very precise cuts within the cytoplasm and the nucleus could be performed without any collateral damage at very low average powers, as low as 7 mW, when using 12 fs laser pulses. Videotaping revealed the formation of some small microbubbles with a lifetime of less than 2 s. When increasing the power up to 20 mW, more destructive effects occurred, due to the occurrence of several bubbles with sizes up to 5 μm. The most efficient way to destroy a single cell of interest was found by scanning the whole cell for a few seconds.

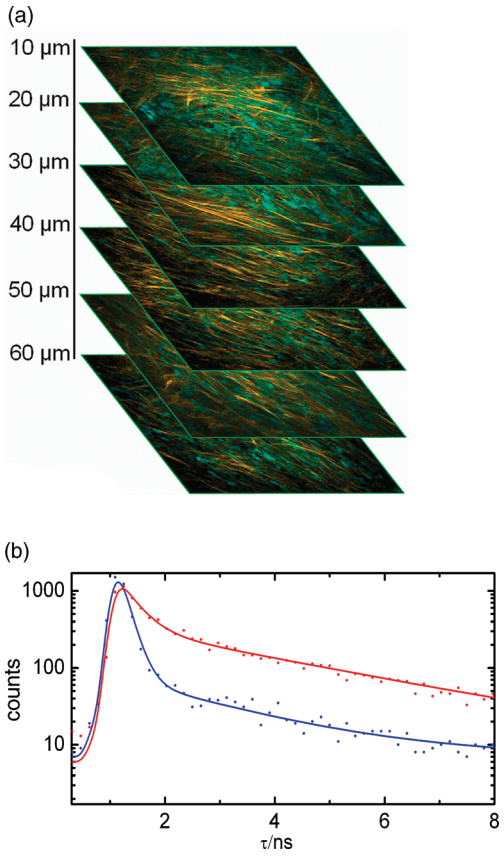

Figure 1.9 (a) Multiphoton sections of stem cell spheroids after chondrogenic differentiation (SHG: yellow fibrils; autofluorescence: blue/green). (b) luminescence decay curves showing the autofluorescence decay of a single fluorescent organelle (upper curve) and the SHG/autofluorescence decay from a collagen structure (lower curve).

To expose single cells inside the stem cell spheroids, at first 3D two-photon autofluorescence optical sectioning was performed. Optical destruction was carried out by single point illumination within the spheroid. In particular, one cell was exposed with high pulse energy (2.6 nJ) and an exposure time of 10 ms. The laser-exposed cell took up the dead-cell indicator ethidium bromide and appeared as very bright fluorescent single cell at the depth of 20 µm.

The method of selective optical destruction of cells of interest can be described as optical knock out [60]. The method has been used to demonstrate the possibility of "optical cleaning" of cell cultures. Stem cell cultures were cleaned in such a way that a particular cell of interest remained alive while the surrounding cells obtained a lethal laser exposure. Figure 1.10 demonstrates the procedure. To isolate a single cell of interest, the surrounding cells within a $0.7 \times 0.7\,\mathrm{mm}^2$ area were exposed

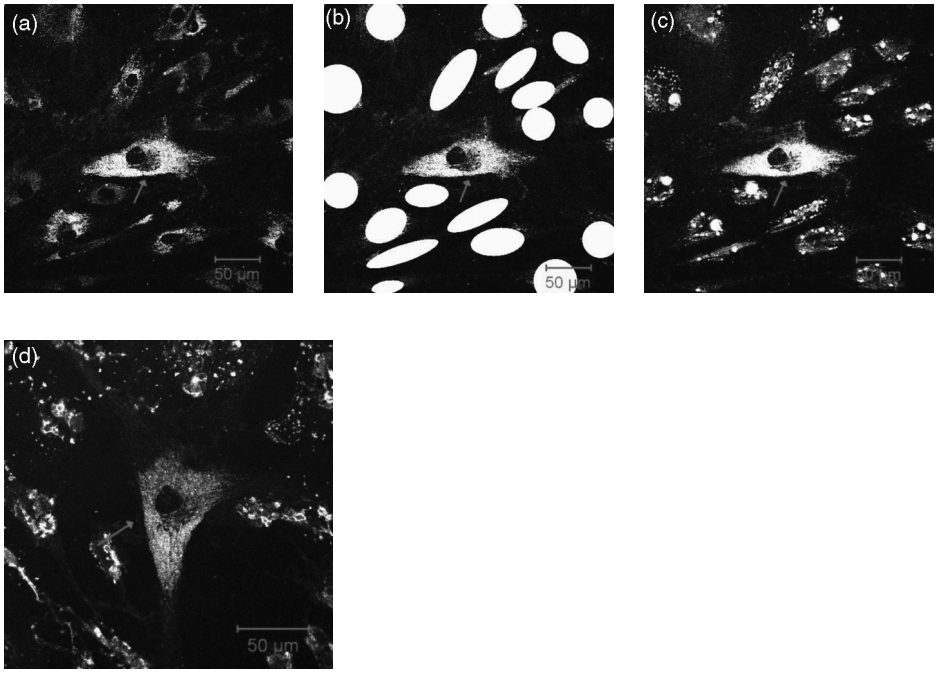

Figure 1.10 Optical cleaning of stem cell cultures. (a) Autofluorescence image before optical knock-out; (b) determination of regions of interest (white), which should be exposed with an intense laser beam at TW cm^{-2} intensity; (c) autofluorescence image taken 1 min after optical knock-out; (d) image after one day. The cells without intense laser exposure survived whereas the surrounding exposed cells were destroyed.

with 200 mW average power and ROI scanning. Significant changes of the morphology and the autofluorescence pattern of the laser exposed cells were monitored within seconds of the intense laser exposure. The non-exposed cell remained intact and was monitored over several days. A normal division of the isolated single living cell was detected as well as the migration of new cells to the laser-exposed area.

The contact-free and chemical-free nanoprocessing method was also probed to realize targeted transfection of single stem cells. For that purpose, single point illumination was performed when opening the shutter for 50 ms, which corresponds to 3.75 million pulses. Figure 1.11 shows two-photon images of an optoporated cell after introduction of the membrane-impermeable GFP plasmid pEGFP-N1 from Clontech (4.7 kb, molar weight 3 MDa) and after cell division occurred. The formation of green fluorescent proteins with an emission maximum at 507 nm was monitored. Interestingly, all laser-exposed cells survived. The green fluorescent daughter cells indicate the successful GFP biosynthesis after introduction of the plasmid into the cytoplasm through the nanopore and the uptake into the cellular DNA as well as the successful reproduction of laser-exposed cells.

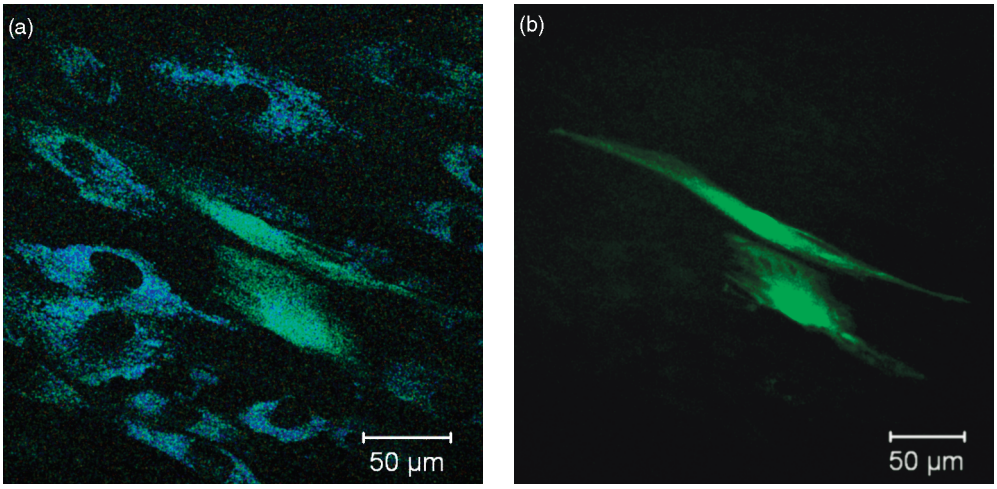

Figure 1.11 Transfection of targeted salivary gland stem cell in an adherent cell culture. A single cell was optoporated. The transfected cell successfully divided and became two-green fluorescent daughter cells. (a) NAD(P)H fluorescence (blue/green) and GFP fluorescence (green) appeared when excited at 750 nm. (b) 800 nm excitation induced mainly GFP emission.

1.6 Discussion and Conclusion

Marker-free multiphoton autofluorescence/SHG microscopy has been used to image stem cells and their development into specialized cells up to five weeks after introduction of a differentiation-stimulating medium. Significant changes of the autofluorescence occurred.

During adipogenic differentiation, the blue-shifted emission maximum and the relative increase of the long fluorescence lifetime (τ_2) indicate the increased ratio of bound to free NAD(P)H (Table 1.2). Because there is an overall decrease of the fluorescence intensity during differentiation, the concentration of the reduced form NAD(P)H drops compared to the oxidized from NAD(P) and therefore the oxygen consumption increases. This hypothesis is in accordance with published data [61] that claims a decrease of NAD(P)H/NAD^+ means an increased metabolism. More studies on various stem cells under different types of differentiation are required to understand the exact metabolism during the differentiation process.

In the case of osteogenic and chondrogenic differentiation, SHG can be used to detect the biosynthesis of collagen [59, 62].

As shown, sub-20 fs laser scanning microscopes can be employed for nano-injection and transfection with low mean powers of 5–7 mW (66–93 pJ @ 75 MHz), which is more than one-order less power than in current femtosecond laser

Table 1.2 Autofluorescence parameters of human salivary gland stem cells (hSGSCs) and cells after adipogenic differentiation (adipocytes) measured by 5D multiphoton imaging.

Cells	NAD(P)H fluorescence intensity	Fluorescence maximum (nm)	Flavin fluorescence intensity	NAD(P)H/ flavin	Fluorescence lifetime (ns)	Bound NAD(P)H/ free NAD(P)H
hSGSCs	High	493	High	Low	Short 0.22/2.00	Low $a_2/a_1 = 0.28$
Adipocytes	Low	Blue-shifted 460	Low	High	Long 0.26/2.33	High $a_2/a_1 = 0.50$

nanoprocessing tools. The use of a low sub-10 mW power level avoids destructive thermal effects and trapping effects and leads to high transfection efficiencies. The potential use of such low power systems opens the way for the manufacturing of ultracompact low-power laser systems for nanoprocessing as well as for imaging at a lower price than current femtosecond laser microscopes.

Stem cells are now at the "bench to bedside" stage for the treatment of myocardial infarction, neurological diseases such as Alzheimer and Parkinson, diabetes, and cancer. Current stem cell therapy is based on adult stem cells where the recruitment of the limited number and their restricted locations is extremely difficult. Furthermore, the stem cells of the patient with genetically based diseases will also carry the genetic effect. There is a hope that multiphoton imaging and nanoprocessing tools can be employed to trace and to manipulate the stem cells as well as to monitor and to influence the differentiation process. However, future work on a large number of different stem cells within their native tissue environment has to be conducted to answer the question of whether the rare stem cells can be identified due to their characteristic autofluorescence behavior. One recent paper reports on the prospective isolation of bronchiolar stem cells from facultative transit-amplifying cells by autofluorescence detection [63]. Results from frozen tissue sections have also demonstrated a different autofluorescence behavior of stem cells in the hair follicle bulge compared to the surrounding cells [64]. Multiphoton microscopes have also been used to monitor the migration of neural stem/progenitor cells in the brain of mice [65].

Current multiphoton microscopes enable the study of stem cells *in vitro*. However, the first two-photon tomographs for skin imaging are in clinical use [2]. There is a chance to trace adult stem cells in the basal cell layer of the epidermis and along the hair shafts. In the near future, two-photon microendoscopes will be available [66] that can be employed to trace stem cells inside the body.

As demonstrated, a multiphoton system cannot only be employed as a high-contrast and high-resolution imaging system but also as highly precise nanoprocessing tool, for example, or optical cleaning and targeted transfection [60, 67, 68]. The optical generation of transient nanoholes will open up a novel way to deliver not only foreign DNA but also other different molecules and chemicals such as RNA, recombinant proteins, nanoparticles, and drugs into the living cell without destructive collateral effects. Very recently it has been demonstrated that the microscope FemtOgen can be employed to deliver super quencher molecular beacon (SQMB) probes into living cells [69].

Future engineering work may result in the development of fiber-based systems with automatic miniaturized high-throughput femtosecond laser systems, for example [70].

In conclusion, multiphoton femtosecond laser systems open up new opportunities in the investigation of human stem cells and their medical application. They can provide morphological and biochemical information with single molecule sensitivity of stem cells in their native environment and can be used to transfect, knock-out, and sort the cells.

References

1 Denk, W., Strickler, J.H., and Webb, W.W. (1990) Two-photon laser scanning microscope. *Science*, **248**, 73–76.

2 König, K. (2008) Clinical multiphoton tomography. *J. Biophoton.*, **1**, 13–23.

3 Maximow, A. (1909) Der Lymphozyt als gemeinsame Stammzelle der verschiedenen Blutelemente in der embryonalen Entwicklung und im postfetalen Leber der Säugetiere. *Folia Haematol.*, **8**, 125–141.

4 Siminovitch, L., McCulloch, E.A., and Till, J.E. (1963) The distribution of colony-forming cells among spleen colonies. *J. Cell Physiol.*, **62**, 327–336.

5 Martin, G.R. (1981) Isolation of a pluripotent cell line from early mouse embryos cultured in medium conditioned by teratocarcinoma stem cells. *Proc. Natl. Acad. Sci. USA*, **78** (12), 7634–7638.

6 Evans, M.J. and Kaufman, M.H. (1981) Establishment in culture of pluripotential cells from mouse embryos. *Nature*, **292**, 154–156.

7 Thomson, J.A., Itskovitz-Eldor, J., Shapiro, S.S., Waknitz, M.A., Swiergiel, J.J., Marshall, V.S., and Jones, J.M. (1998) Embryonic stem cell lines derived from human blastocysts. *Science*, **282**, 1145–1147.

8 Gärtner, W., Gröbler, B., Schubert, D., Wabnitz, H., and Wilhelmi, B. (1988) Fluorescence scanning microscopy combined with subnanosecond time resolution. *Exp. Tech. Phys.*, **36**, 443–451.

9 König, K. (1989) PhD thesis. Optical cancer diagnosis and picosecond fluorescence lifetime microscopy. Archive of the Friedrich Schiller University Jena.

10 Bugiel, I., König, K., and Wabnitz, H. (1989) Investigations of cells by fluorescence laser scanning microscopy with subnanosecond time resolution. *Laser Life Sci.*, **3**, 47–53.

11 Hänninen, P.E., Soini, E., and Hell, S.W. (1994) Continuous wave excitation two-photon fluorescence microscopy. *J. Microsc.*, **176**, 222–225.

12 König, K., Liang, H., Berns, M.W., and Tromberg, B.J. (1995) Cell damage by near-IR microbeams. *Nature*, **377**, 20–21.

13 König, K., Liang, H., Berns, M.W., and Tromberg, B.J. (1996) Cell damage in near infrared multimode optical traps as a result of multiphoton absorption. *Opt. Lett.*, **21**, 1090–1092.

14 König, K. (2000) Multiphoton microscopy in life sciences. *J. Microsc.*, **200**, 83–104.

15 Squirrel, J.M., Wokosin, D.L., White, J.G., and Bavister, B.D. (1999) Long-term two-photon fluorescence imaging of mammalian embryos without compromising viability. *Nat. Biotechnol.*, **17**, 763–767.

16 Fischer, F., Beate, V., Puschmann, S., Greinert, R., Breitbart, E., Kiefer, J., and Wepf, R. (2008) Assessing the risk of skin damage due to femtosecond laser irradiation. *J. Biophoton.*, **1** (6), 470–477.

17 Rebecca, M.W., Warren, R.Z., and Watt, W.W. (2001) Multiphoton microscopy in biological research. *Curr. Opin. Chem. Biol.*, **5**, 603–608.

18 Zipfel, W.R., Williams, R.M., and Webb, W.W. (2003) Nonlinear magic: multiphoton microscopy in the biosciences. *Nat. Biotechnol.*, **21**, 1369–1377.

19 König, K. and Schneckenburger, H. (1994) Laser-induced autofluorescence for medical diagnosis. *J. Fluoresc.*, **4**, 17–40.

20 Freund, I. and Deutsch, M. (1996) 2nd harmonic microscopy of biological tissue. *Opt. Lett.*, **11**, 94–96.

21 Masters, B.R., So, P.T., and Gratton, E. (1997) Multiphoton excitation fluorescence microscopy and spectroscopy of *in vivo* human skin. *Biophys. J.*, **72**, 2405–2412.

22 Zoumi, A., Yen, A., and Tromberg, B.J. (2002) Imaging cells and extracellular matrix in vivo by using second harmonic generation and two-photon excited fluorescence. *Proc. Natl. Acad. Sci. USA*, **99**, 11014–11019.

23 König, K., Schenke-Layland, K., Riemann, I., and Stock, U.A. (2005) Multiphoton autofluorescence imaging of

intratissue elastic fibers. *Biomaterials*, **26**, 495–500.

24 Cox, G., Moreno, N., and Feijo, J. (2005) Second harmonic imaging of plant polysaccharides. *J. Biomed. Opt.*, **10**, 024013.

25 Chance, B., Schoener, B., Oshino, R., Itshak, F., and Nakase, Y. (1979) Oxidation-reduction ratio studies of mitochondria in freeze-trapped samples. *J. Biol. Chem.*, **254**, 4764–4771.

26 Huang, S., Ahmed, A., Heikal, A., and Webb, W.W. (2002) Two-photon fluorescence spectroscopy and microscopy of NAD(P)H and flavoproteins. *Biophys. J.*, **82**, 2811–2825.

27 Niesner, R., Peker, B., Schlüsche, P., and Gericke, K.H. (2004) Noniterative bi-exponential fluorescence lifetime imaging in the investigation of cellular metabolism by mean of NAD(P)H autofluorescence. *Phys. Chem. Chem. Phys.*, **5** (8), 1141–1149.

28 Dimitrow, E., Riemann, I., Ehles, A., Koehler, J., Norgauer, J., Elsner, P., König, K., and Kaatz, M. (2009) Spectral fluorescence lifetime detection and selective melanin imaging by multiphoton laser tomography for melanoma diagnosis. *Exp. Dermatol.*, **18** (6), 509–515.

29 Vogel, A., Noack, J., Hüttman, G., and Paltauf, G. (2005) Mechanisms of femtosecond laser nanosurgery of cells and tissues. *Appl. Phys. B*, **81**, 1015–1047.

30 König, K., Becker, T.W., Fischer, P., Riemann, I., and Halbhuber, K.J. (1999) Pulse-length dependence of cellular response to intense near-infrared laser pulses in multiphoton microscopes. *Opt. Lett.*, **24**, 113–115.

31 König, K., Riemann, I., and Fritzsche, W. (2001) Nanodissection of human chromosomes with near infrared femtosecond laser pulses. *Opt. Lett.*, **26**, 819–821.

32 König, K., Riemann, I., Fischer, P., and Halbhuber, K.J. (1999) Intracellular nanosurgery with near infrared femtosecond laser pulses. *Cell Mol. Biol.*, **45**, 195–201.

33 König, K. (2000) Robert Feulgen prize lecture 2000. Laser tweezers and multiphoton microscopes in life sciences. *Histochem. Cell Biol.*, **114**, 79–92.

34 König, K., Riemann, I., Stracke, F., and Le Harzic, R. (2005) Nanoprocessing with nanojoule near-infrared femtosecond laser pulses. *Med. Laser Appl.*, **20**, 169–184.

35 Tirlapur, U.K. and König, K. (2002) Targeted transfection by femtosecond laser. *Nature*, **418**, 4295–4298.

36 Watanabe, W., Matsunaga, S., Shimada, T., Higashi, T., Fukui, K., and Itoh, K. (2005) Femtosecond laser disruption of mitochondria in living cells. *Med. Laser Appl.*, **20**, 185–191.

37 Heisterkamp, A., Maxwell, I.Z., Mazur, E., Underwood, J.M., Nickerson, J.A., Kumar, S., and Ingber, D.E. (2005) Pulse energy dependence of subcellular dissection by femtosecond laser pulses. *Opt. Express*, **13**, 3690–3696.

38 Shimada, T., Watanabe, W., Matsunaga, S., Higashi, T., Ishii, H., Fukui, K., Isobe, K., and Itoh, K. (2005) Intracellular disruption of mitochondria in a living HeLa cell with a 76-MHz femtosecond laser oscillator. *Opt. Express*, **13**, 9869–9880.

39 Sacconi, L., Tolic-Norrelykke, I., Antolini, R., and Pavone, F.S. (2005) Combined intracellular three-dimensional imaging and selective nanosurgery by a nonlinear microscope. *J. Biomed. Opt.*, **10**, 14002.

40 König, K., Krauss, O., and Riemann, I. (2002) Intratissue surgery with 80MHz nanojoule femtosecond laser pulses in the near infrared. *Opt. Express*, **10**, 171–176.

41 Pittenger, M.F., Mackay, A.M., Beck, S.C., Jaiswal, R.K., Douglas, R., Moska, J.D., Moorman, M.A., Simonetti, D.W., Craig, S., and Marshak, D.R. (1999) Multilineage potential of adult human mesenchymal stem cells. *Science*, **284**, 143–147.

42 Sakaguchi, Y., Sekiya, I., Yagishita, K., and Muneta, T. (2005) Comparison of human stem cells derived from various mesenchymal tissues: superiority of synovium as a cell source. *Arthritis Rheum.*, **52**, 2521–2529.

43 Sauer, H., Rahimi, G., Hescheler, J., and Wartenberg, M. (1999) Effects of electrical fields on cardiomyocyte differentiation of embryonic stem cells. *J. Cell Biochem.*, **75**, 710–723.

44 Zou, G.-M., Chen, J.-J., and Ni, J. (2006) Light induces differentiation of mouse embryonic stem cells associated with

activation of ERK5. *Oncogene*, **25**, 463–469.

45 Wagner, D.R., Lindsey, D.P., Li, K.W., Tummala, P., Chandran, S.E., Smith, R.L., Longaker, M.T., Carter, D.R., and Beaupre, G.S. (2008) Hydrostatic pressure enhances chondrogenic differentiation of human bone marrow stromal cells in osteochondrogenic medium. *Ann. Biomed. Eng.*, **36**, 813–820.

46 Ge, D., Liu, X., Wu, J., Tu, Q., Shi, Y., and Chen, H. (2009) Chemical and physical stimuli induce cardiomyocyte differentiation from stem cells. *Biochem. Biophys. Res. Commun.*, **381**, 317–321.

47 Suwa, T., Yang, L., and Hornsby, P.J. (2001) Telomerase activity in primary cultures of normal adrenocortical cells. *J. Endocrinol.*, **170**, 677–684.

48 Oh, B.-K., Lee, C.-H., Park, C., and Park, Y.N. (2004) Telomerase regulation and progressive telomere shortening of rat hepatic stem-like epithelial cells during *in vitro* aging. *Exp. Cell Res.*, **298**, 445–454.

49 Ju, Z. and Rudolph, K.L. (2006) Telomeres and telomerase in stem cells during aging and disease. *Genome Dyn.*, **1**, 84–103.

50 Rubio, D., Garcia-Castro, J., Martin, M.C., Fuente, R., Cigudosa, J., Lloyd, A.C., and Bernad, A. (2005) Spontaneous human adult stem cell transformation. *Cancer Res.*, **65**, 3035–3039.

51 Bruder, S.P., Jaiswal, N., and Haynesworth, S.E. (1997) Growth kinetics, selfrenewal, and the osteogenic potential of purified human mesenchymal stem cells during extensive subcultivation and following cryopreservation. *J. Cell Biochem.*, **64**, 278–294.

52 Chung, S., Shin, B.-S., Hedlund, E., Pruszak, J., Ferree, A., Kang, U.J., Isacson, O., and Kim, K.-S. (2006) Genetic selection of sox1GFP-expressing neural precursors removes residual tumorigenic pluripotent stem cells and attenuates tumor formation after transplantation. *J. Neurochem.*, **97**, 1467–1480.

53 Schenke-Layland, K., Riemann, I., Damour, O., Stock, U.A., and König, K. (2006) Two-photon microscopes and *in vivo* multiphoton tomographs - Powerful diagnostic tools for tissue engineering and drug delivery. *Adv. Drug Deliv. Rev.*, **58**, 878–896.

54 Takahashi, K., Tanabe, K., Ohnuki, M., Narita, M., Ichisaka, T., Tomoda, K., and Yamanaka, S. (2007) Induction of pluripotent stem cells from adult human fibroblasts by defined factors. *Cell*, **131**, 861–872.

55 Becker, W. (ed.) (2005) *Advanced Time-Correlated Single-Photon Counting Techniques*, Springer, Berlin, Heidelberg, New York.

56 Periasamy, A. (ed.) (2001) *Methods in Cellular Imaging*, Oxford University Press, Oxford, New York.

57 Periasamy, A. and Clegg, R.M. (eds) (2009) *FLIM Microscopy in Biology and Medicine*, Taylor and Francis Group (CRC Press), Roca Raton, London, New York.

58 Diskinson, M.E., Bearman, G., Tille, S., Landsford, R., and Fraser, S.E. (2001) Multi-spectral imaging linear unmixing add a whole new dimension to laser scanning fluorescence microscopy. *BioTechniques*, **31**, 1272–1278.

59 Uchugonova, A. and König, K. (2008) Two-photon autofluorescence and second-harmonic imaging of adult stem cells. *J. Biomed. Opt.*, **13**, 054068.

60 Uchugonova, A., Isemann, A., Gorjup, E., Tempea, G., Bückle, R., Watanabe, W., and König, K. (2008) Optical knock out of stem cells with extremely ultrashort femtosecond laser pulses. *J. Biophoton.*, **1**, 463–469.

61 Guo, H.-W., Chen, C.-T., Wei, Y.-H., Lee, O.K., Gukassyan, V., Kao, F.-J., and Wang, H.-W. (2008) Reduced nicotinamide adenine dinucleotide fluorescence lifetime separates human mesenchymal stem cells from differentiated progenies. *J. Biomed. Optic. Lett.*, **13**, 050505(1-3).

62 Lee, H.S., Teng, S.W., Chen, H.C., Lo, W., Sun, Y., Lin, T.Y., Chiou, L.L., Jiang, C.C., and Dong, C.Y. (2006) Imaging the bone marrow stem cells morphogenesis in PGA scaffold by multiphoton autofluorescence and second harmonic (SHG) imaging. *Tissue Eng.*, **12**, 2835–2842.

63 Teisanu, R.M., Lagasse, E., Whitesides, J.F., and Stripp, B.R. (2009) Prospective isolation of bronchial stem cells based upon immunophenotypic and autofluorescence characteristic. *Stem Cells*, **27**, 612–622.

64 Wu, B.P., Tao, Q., and Lyle, S. (2005) Autofluorescence in the stem cell region of the hair follicle bulge. *J. Invest. Dermatol.*, **124**, 860–862.

65 Zhao, L.-R. and Nam, S.C. (2007) Multiphoton microscope imaging: the behavior of neural progenitor cells in the rostral migratory stream. *Neurosci. Lett.*, **425**, 83–88.

66 König, K., Weinigel, M., Hoppert, D., Bückle, R., Schubert, H., Köhler, M.J., Kaatz, M., and Elsner, P. (2008) Multiphoton tissue imaging using high-NA microendoscopes and flexible scan heads for clinical studies and small animal research. *J. Biophoton.*, **1**, 506–513.

67 Uchugonova, A., König, K., Bückle, R., Isemann, A., and Tempea, G. (2008) Targeted transfection of stem cells with sub-20fs laser pulses. *Opt. Express*, **16**, 9357–9364.

68 Uchugonova, A., Müller, J., Bückle, R., Tempea, G., Isemann, A., Stingl, A., and König, K. (2008) Negatively-chirped laser enables nonlinear excitation and nanoprocessing with sub 20fs pulses. *Proc. of SPIE*, **6860**, 686015.

69 Földes-Papp, Z., König, K., Studier, H., Bückle, R., Breunig, H.G., Uchugonova, A., and Kostner, G.M. (2009) Trafficking of mature miRNA into the nucleus of life liver cells. *Curr. Pharm. Biotechnol.*, **10** (6) 569–578.

70 Tsampoula, X., Garces-Chavez, V., Comrie, M., Stevenson, D.J., Agate, B., Brown, C.T.A., Gunn-Moore, F., and Dholakia, K. (2007) Femtosecond cellular transfection using a nondiffracting light beam. *Appl. Phys. Lett.*, **91**, 053902.